Book of Tutorials and Abstracts

European Microbeam Analysis Society

EMAS 2025

18th

EUROPEAN WORKSHOP

on

MODERN DEVELOPMENTS AND APPLICATIONS IN MICROBEAM ANALYSIS

11 to 15 May 2025
at the
TecnoCampus
Mataró (Barcelona), Spain

Organized in collaboration with the
Universitat de Barcelona, Spain

EMAS
European Microbeam Analysis Society eV
www.microbeamanalysis.eu/

This volume is published by:
European Microbeam Analysis Society eV (EMAS)
EMAS Secretariat
c/o Eidgenössische Technische Hochschule, Institut für Geochemie und Petrologie
Clausiusstrasse 25
8092 Zürich
Switzerland

ISBN 978 90 8227 6985
NUR code: 972 – Materials Science

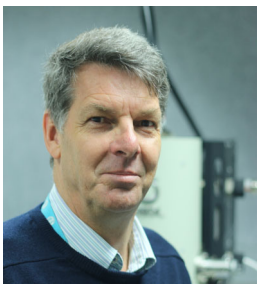

DEVELOPMENT AND APPLICATION OF SOFT X-RAY SPECTROSCOPY AND CATHODOLUIMINESCENCE

C.M. MacRae[1,*], N.C. Wilson[1], A. Torpy[1], M.A. Glenn[1], A.G. Salek[2], Z. Pintér[1], A.G. Tomkins[3] and D.G. McCulloch[2]

1 CSIRO Mineral Resources, Microbeam Laboratory
AU-3169 Clayton South, Victoria, Australia
2 RMIT University, School of Science, Physics
Melbourne, Victoria, Australia
3 Monash University, School of Earth, Atmosphere and Environment
Melbourne, Victoria, Australia
e-mail: colin.macrae@csiro.au

Colin is a senior principal research scientist with the Commonwealth Science Industrial Research Organisation (CSIRO), based in Clayton, Victoria. He is a group leader and directs microanalysis and X-ray diffraction research in the Microbeam Laboratory, which is the key electron beam microcharacterisation facility for Minerals and Mineral Processing problems within CSIRO. Colin has a strong interest in the application of high resolution microanalysis and mapping in the electron microprobe to solve industrial problems related to the minerals industry.

Most recently Colin has been at the forefront of the development of hyperspectral soft X-ray emission spectrometry and analysis and combining this technique with cathodoluminescence together with hyperspectral EDS collection and analysis. With the introduction of this combined technique he has developed new detector systems and analysis procedures so that the both SXES and cathodoluminescence signals can be quickly analysed, the emitting X-rays and ions identified and the emission quantified. To make full use of these techniques he has recently worked on the integration of LN cold stage technology into the EPMA to reduce beam damage.

Colin is a past president of the Australian Microbeam Analysis Society (AMAS). He has also been convenor of three AMAS biennial symposia and organised a MAS topical conference on cathodoluminescence in 2011.

1. ABSTRACT

The addition of hyperspectral soft x-ray emission spectrometers (SXES) and cathodoluminescence (CL) spectrometry to electron microprobes gives access to spectroscopies that provide sample information not available from wavelength-dispersive (WDS) or energy-dispersive X-ray spectrometers (EDS). We have developed software and hardware to allow collection of the backscatter electron signal, WDS, EDS, SXES and CL spectral data simultaneously. This unique strategy enables our instrumentation to avoid pixel misalignment and minimises electron beam induced damage artefacts associated with multiple pass mapping. Originally this approach was developed for a JEOL 8530F-CL and most recently has been implemented on an iHP200F-CL. We have utilised this technology on a range of material and geological problems and here we show firstly an examples of grain orientation information that can be obtained from SXES spectra collected during mapping naturally occurring graphite from a Tanzanian deposit. In addition, a ureilite sample, NWA 7983, has been studied to better understand the formation and presence of lonsdaleite and diamond within these meteorites.

2. INTRODUCTION

A field emission electron probe microanalyser (EPMA) equipped with traditional wavelength- and energy-dispersive X-ray spectrometers, a soft X-ray emission spectrometer (SXES) and a cathodoluminescence (CL) spectrometer has been used to investigate two different mineral samples both containing carbon. Firstly, a carbon rich Epanko deposit located within the Mahenge Inlier in the Eastern Granulite terrane of the East African Orogen [1] and the secondly a ureilite meteorite, NWA7983 [2]. While both samples contained carbon, the first one primarily was composed of carbon in the graphite structure, while the second sample contained carbon in three distinct forms graphite, diamond and lonsdaleite.

In the first sample the rocks consist of anorthosite basement and a sequence of sediments including shales, with variable organic carbon content, and limestones that have been metamorphosed to high temperature and pressure as schists, graphitic schists and marbles. The whole complex was subsequently thrust westwards during the closure of the Mozambique Ocean between 590 and 560 Ma [3]. The sample investigated from this Tanzanian deposit shows the rock is composed of plagioclase and K-feldspar with quartz, biotite, pyrrhotite, and muscovite after sillimanite. One of the aims of this study was to understand the crystallinity and morphology of the carbon, as thermodynamic modelling of metamorphic pressure-temperature conditions indicate that the ore had experienced peak metamorphic conditions of 8.5 kbar and > 750 °C but with a later phase of reworking at 3.5 - 4 kbar and 550 °C. Under the peak metamorphic conditions, the carbon should be fully crystalline graphite. Initial Raman analysis had shown a mixture of signals indicating the possibility of different crystallinities of graphite. X-ray mapping in combination with soft X-ray emission (SXE) spectroscopy was employed to examine the carbon spectroscopy on a polished mount. Previous

carbon spectroscopy studies have shown soft X-ray spectroscopy is sensitive to the type of carbon bonding present [4] and in the case of graphite the crystallographic plane responsible for the emission [5].

The second sample was a ureilite, NWA7983. Ureilites are primitive achondrite meteorites that are residues of fractional melt extracted from deep within a ureilite parent body (UPB) [6]. Most likely the UPB underwent extensive melting and had a diameter that may have been > 530 km [7], it was most likely a dwarf planet, massive enough to form a spheroid under hydrostatic equilibrium, and these meteorites are, therefore, our only large suite of samples from the mantle of such a body. It is known that up to 7 % graphite occurs in all ureilites, abundant diamond occur among graphite in most, and evidence for the presence of lonsdaleite has also been previously reported [6, 8]. Lonsdaleite, named after Kathleen Lonsdale, is a hexagonal form of diamond and has been widely used as a marker of asteroidal impacts [9] and was first reported in 1967 in the Canyon Diablo and Goalpara meteorites [10], and evidence for this phase has also been found in the diffraction signatures in the products of experiments that subjected graphite to static [11] or shock [12] compression. The presence of lonsdaleite within ureilites is still quite contentious and it has recently been suggested that lonsdaleite does not exist as a discrete material in nature (but is instead defective cubic diamond dominated by twinning and stacking faults, given that these defects would produce the diffraction signatures of lonsdaleite) [9]. However, more recent studies have confirmed its rapid production in experiments at 50 GPa, which led to the formation of diamond and lonsdaleite [13, 14]. One of the key challenges in confirming that lonsdaleite exists in nature has been a lack of samples that contain large enough crystallites that can be unambiguously identified. It is also unclear what the formation process was for the various phases of carbon formed in ureilites and the interplay between them. Some diamond/lonsdaleite features are said to be consistent with having formed by shock [8], based on TEM observations that carbon phases are crystallographically related.

3. MATERIALS AND METHODS

3.1. Spectroscopy - graphite

Selected graphite-diamond and graphite-lonsdaleite-diamond-bearing domains were sectioned and prepared as thin sections. Careful grinding and polishing methods enabled the variable hardness materials to be preserved and kept close to optically flat. Prior to examining in the EPMA the samples were coated with 4 - 6 nm of carbon using a Leica ACE600 thin film coater. A JEOL 8530F-CL HyperProbe located at the CSIRO Microprobe Laboratory in Melbourne equipped with wavelength-dispersive (WD) and energy-dispersive (ED) X-ray spectrometry, twin Bruker spectrometers, was used to examine the sections [15]. In addition, the EPMA was equipped with an optical grating spectrometer [16], for cathodoluminescence (CL) collection and analysis, and a JEOL SXES (SS-94000SXES) [17] extensively modified by CSIRO [18]. CL and SXES (soft X-ray emission spectrometry) were used in combination to characterise the

textural associations between the various forms of carbon (graphite, diamond and lonsdaleite), producing maps characterising the key textures. The optical spectrometer collected from 199 to 972 nm and had a 200 nm entrance slit, producing an effective resolution of 6.7 nm. The light optics of the EPMA had been extensively modified, by CSIRO, to maximise the overall transmission with a focus on UV. The spectrometer was operated in a temperature-controlled chamber to minimise temperature fluctuations of the ADC electronics in the spectrometer, this minimises the need for dark current corrections across maps. The enclosure was maintained to ± 0.1 °C.

The SXES was equipped with both JS50XL and JS200N gratings, with the latter used in these studies. For the Tanzanian samples the SXES used equipped with a Princeton PIXIS 2048B CCD, with 13.5 µm pixels, operated at 100 kHz ADC readout mode to maximise signal-to-noise performance of the spectrometer [19]. The readout time of the CCD at 100 kHz is 340 ms, which is different from dead-time as the CCD continues to acquire during read out. The CCD was subsequently upgraded to a Princeton Sophia which has a quad amplifier readout enabling the 2048 × 2048 array of pixels to be divided into four and read in parallel. The low noise and relatively large pixel size of this CCD, 15 µm, makes this a sensitive camera to soft X-rays, highly stable and able to operate at faster readout rates, of down to 40 ms. The PIXIS CCD was operated at -60 °C while the Sophia CCD at -90 °C and in all cases during mapping the EPMA had a LN_2 cold trap in operation to minimise ice build-up on the CCD surface, base pressure of the vacuum system is 1×10^{-6} Torr. The LN_2 trap was automatically filled using a special cryogenic liquid filling system developed by Norhof, allowing continuous operation of cold trap for up to 6 days using a 50 L dewar. In all maps a JS200N grating was used, and the CCD was mounted using an offset flange resulting in a typical energy range of 38 - 142 eV. The SXES was calibrated using C-K 3rd to 7th, Al-L 1st, and Zr-Mζ 2nd and 3rd order reflections and a 5th order polynomial was used to fit the measurements. The energy resolution at the Al-L Fermi edge as measured between 75 % and 25 % of the peak height was 105 meV. A spectral examination of the C-Kα line on highly oriented pyrolytic graphite (HOPG) found that the higher the order of the reflection, the greater the resolution. However, as the order of reflection increased the intensity decreased. The second order reflection offered the best compromise between resolution and signal-to-noise ratio, Figs. 1a and 1b. A long dark background spectrum was acquired on the SXES prior to mapping and subtracted from every pixel to remove spectral shapes introduced by the non-uniformity in the CCD background and the associated electronics. Typically, 2,000 - 3,000 spectra were acquired for the long dark spectrum and spectra with spikes greater than 5σ deviation were rejected. In addition, the temperature response of the CCD electronics was tracked by measuring the blanked off pixels on the CCD and using a fast Fourier transform (FFT) to produce a further background correction to room temperature variations in the electronics. The SXES was controlled using inhouse software and both the CL and SXES systems were slaved to the EPMA through a combination of hardware and software control. At the completion of mapping each set of hyperspectral data (EDS, CL and SXES) together with WDS and electron signals were concatenated into a single map file. These were then processed with inhouse software, CHIMAGE [20].

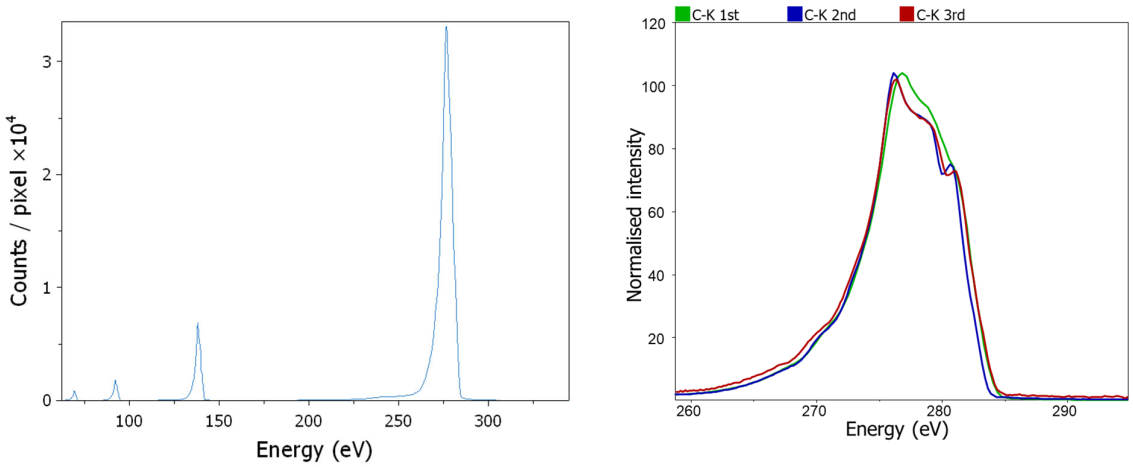

Figure 1 a) SXES spectra from a graphite particle within the Tanzanian sample showing the C-Kα 1st, 2nd, 3rd and 4th order reflections. The higher order reflections show decreasing intensity and when normalised in b), shows the C-Kα 1st (green), 2nd (blue) and 3rd (red) order reflections the greater the order of the reflection, the better the resolution. The second order reflection shows enhanced resolution and offers the best compromise between sensitivity and resolution.

Analysis conditions were varied with 7 - 10 kV accelerating voltage, 80 - 100 nA [20] beam current, and a dwell per pixel of 400 ms, and maps were collected by scanning the stage with a matching step size and spot size ranging from 0.5 - 2.0 µm. The low accelerating voltage is ideal for exciting carbon X-rays and offers a sub-micrometre analytical interaction volume. Thresholding of the CL spectra allowed integration with element maps to highlight the relative distribution of graphite, diamond, and lonsdaleite among silicates. Diamond is distinguished from lonsdaleite by their respective features in the CL spectral response, which makes imaging their relative distribution straightforward. The CL peak at 2.157 eV was selected as being characteristic of diamond, whereas the peak at 2.317 eV was selected to highlight lonsdaleite in the maps of the ureilites examined. The SXES spectrum provides supporting evidence for the presence of lonsdaleite as we see that the carbon X-ray peak shape is always narrower than diamond which is supported by quantum mechanical modelling.

3.2. Modelling

Molecular orbital calculations were carried out using the CRYSTAL ab initio software package [21]. The basis set used for carbon was a 6-111G* type which was optimised for graphite [5], and the B3LYP functional was used for the treatment of electron exchange and correlation [22]. Reciprocal space integration was performed by using and 12×12×12 Monkhorst-Pack mesh [23]. The electron density of states was calculated using the Fourier-Legendre technique as implemented in the CRYSTAL software and were then further convoluted with a 0.9 eV Gaussian to simulate the SXES response for the C-Kα transition.

4. RESULTS AND DISCUSSION

4.1. Tanzanian deposit - Carbon as graphite

4.1.1. Sample mineralogy. The phases present in the sample were determined by clustering the X-ray hyperspectral map, both ED and WD data, which was collected in parallel to the CL and SXES data, and then analysing the spectra associated each cluster [24]. From the analyses, the minerals were identified and then labelled, Fig. 2a. The sample is dominated by quartz (SiO_2), graphite, K-feldspar ($KAlSi_3O_8$), biotite ($K[Mg,Fe]_3[AlSi_3O_{10}(OH,F)_2]$), muscovite ($KAl_2(Si_3Al)O_{10}(OH,F)_2$), plagioclase ($(Na,Ca)(Si,Al)_4O_8$) and pyrite ($FeS_2$). The graphite grains often appear to have formed with pyrite which may reflect the reducing conditions associated with the formation of graphite. The presence of both together suggests that the rock was originally sediment that contained organic matter [25].

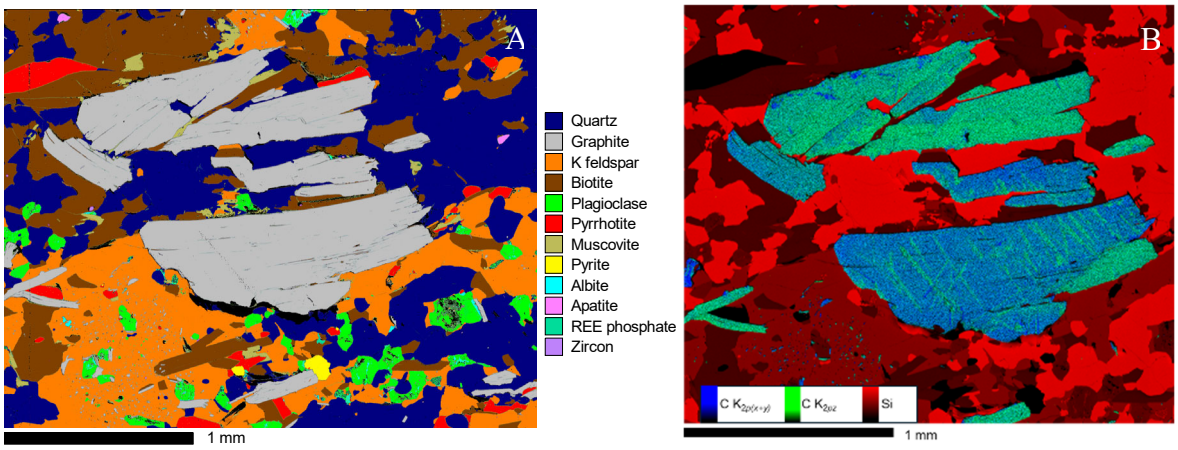

Figure 2. a) Phase patched map showing carbon grains surrounded by silicates and sulphides from a Tanzanian deposit. b) Peak fitted carbon spectra were selected to highlight the C-K $2p(x+y)$ and $2pz$ together with Si-K. The C-K was measured using the SXES and the JS200N grating while the Si-K was measured by WDS.

4.1.2. Graphite. C Kα spectra from distinctively different carbon-rich grains, measured using the SXES, are shown in Fig. 3a. The graphite spectra are similar to those observed from HOPG graphite and attributed to $2p(x+y)$ and $2pz$ orbitals. The two polarisations in graphite spectra have been previously reported by Holliday and Terauchi *et al.* [26, 27]. The C-Kα 2nd order peak at 281 eV is attributed to π-bonding, while the peak at 271 eV is attributed to σ-bonding. The presence of π- and σ-bonding indicates the highly crystalline graphitic nature of the carbon as these would not be present if it was amorphous. The difference in the spectral shapes reflects the orientation of the individual grains as the SXES is highly sensitive to crystal or in this case grain orientation. Either by selecting several energy regions across the C-Kα peak and projecting these across the mapped area, the different orientations can be seen. A better way to show the

grain orientation is to fit a series of Gaussians to each of the end-member orientations and then lock the peak shapes but allow the overall height to move freely. The sum of the Gaussians is a close match to the spectra shape. When each pixel in the map is fitted with the two peak shapes, defined by the Gaussian sets, the resulting map is given in Fig. 2b.

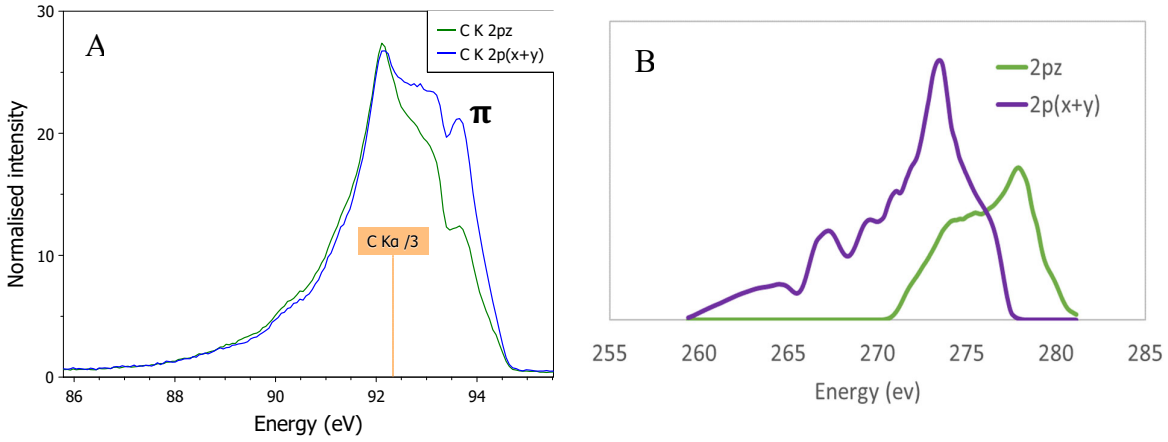

Figure 3. a) 3rd order C-K spectra collected from the two different grain orientations, dominated by 2*pz* and 2*p*(*x*+*y*) respectively, in the mapped region, Fig 2. The 2*pz* shows the π-bond, in graphite. Both these C-K spectra are observed in graphite. b) Calculated DOS for graphite showing the pure 2*pz* and 2*p*(*x*+*y*).

The two calculated density of states (DOS) for graphite showing the pure 2*pz* and 2*p*(*x*+*y*) are given in Fig. 3b. The 2*pz* is dominated by the π-bonding. By taking a percentage of each of the 2*pz* and the 2*p*(*x*+*y*) we can sum them and generate different orientations of grains to the beam. This has been done for the two main orientations observed in the sample shown, in Fig 2b. These projections are shown in Figs. 4a and 4b. Figure 4 shows both the sum of the DOS and the effective orientation of the graphite to the beam. This is a simple and powerful means of measuring grain orientation and has approximately 1 % error in the orientation. The sample preparation is also much simpler than for EBSD especially for graphite which really requires ion beam milling for good Kikuchi patterns.

4.2. Ureilite meteorite - Carbon as graphite, diamond and lonsdaleite

Ureilites are a distinct class of achondrite meteorites, commonly believed to have been ejected from their parent body following a catastrophic impact event in the early solar system [6, 28]. Ureilites are predominantly composed of pigeonite [$(Mg,Fe^{2+},Ca)(Mg,Fe^{2+})Si_2O_6$], olivine [$(Mg,Fe)_2SiO_4$] and low-calcium pyroxene, with smaller amounts of FeNi metal and troilite [FeS]. Augite, chrome spinel and plagioclase are less commonly found. Ureilites typically contain up to 7 % carbon [29], higher than most other achondrites and even some primitive carbonaceous chondrites. A wide range of coexisting carbon phases have been reported,

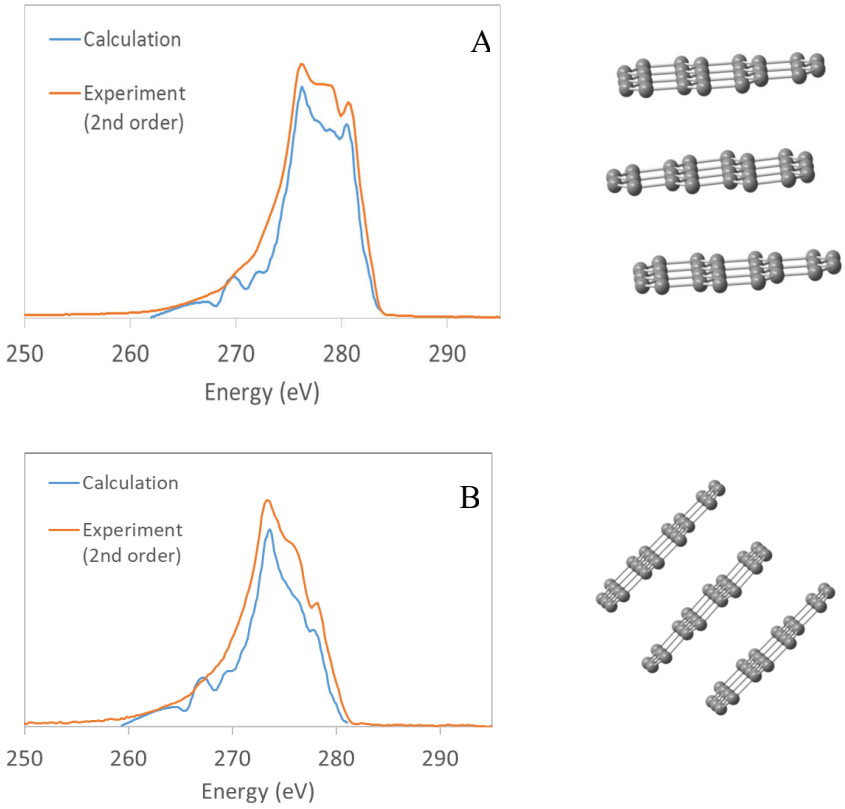

Figure 4. a) Comparison between the C-K 2nd order reflection from the green grains, Fig. 2, compared to both the calculated DOS 2*pz* and 2*p*(*x*+*y*). The best fit provides the angle of the planes, and this is seen in the associated projection of the carbon atoms. In this case the grain is almost pure 2*pz*. b) The blue grains, Fig. 2, C-K 2nd order reflection shows these grains are closer to 45° comprising almost equal parts of 2*pz* and 2*p*(*x*+*y*).

including amorphous carbon, graphite [6], diamond [30], lonsdaleite [6, 31] and defective diamond-like structures [32]. However, the mechanisms responsible for the formation of these phases are not fully understood. The presence of lonsdaleite in ureilites is controversial and researchers are actively examining both natural and synthetically produced materials to understand the formation mechanisms. We have used a combination of CL and SXES together with DOS calculations to better understand the formation mechanisms. Here we focus on the Northwest Africa (NWA) sample, NWA7983 [32], Fig. 5, to better understand the different carbon forms.

In this sample we have used the CL collected during mapping to differentiate the diamond and from the lonsdaleite as they have distinct CL signatures. This can be done relatively quickly as the CL signal is quite strong. In parallel to SXES measurements we have performed theoretical calculations with CRYSTAL an ab initio software package [33] and the resulting calculations (Fig. 6) show the difference between cubic diamond where the carbon 2*px*, 2*py* and 2*pz* orbitals have identical energy levels while in lonsdaleite the 2*pz* DOS differs from the identical 2*px* and 2*py* DOS.

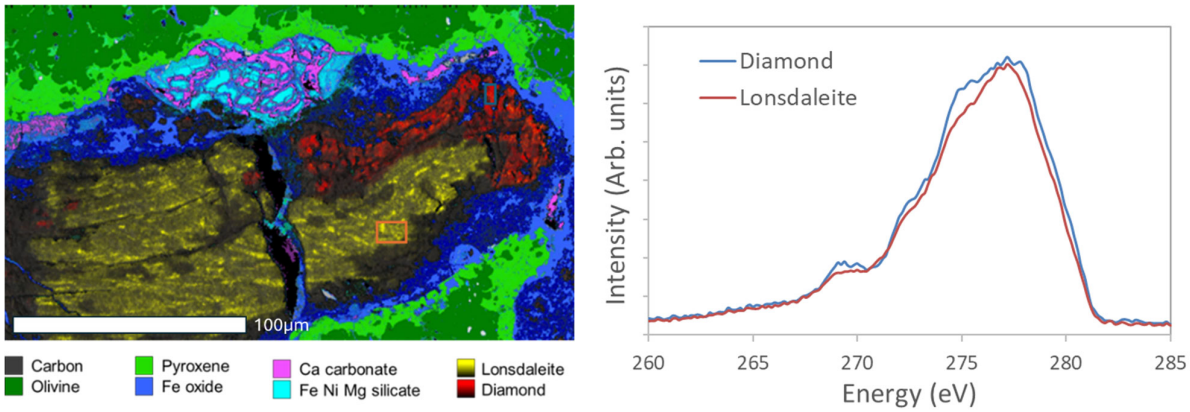

Figure 5. a) Phase patched map from selected region on NWA7983 showing a relatively large lonsdaleite grain, 200 µm, intergrown with diamond. The phases identified from the X-rays were olivine, pyroxene, iron oxide, Ca-carbonate, (Fe,Ni,Mg) silicate, while diamond and lonsdaleite were identified by CL. b) Selected spectra collected using JS200N grating, C-K 4th order reflection, from orange square, lonsdaleite, and blue square, diamond, are shown. The C-K 4th order spectral shapes are similar, however, lonsdaleite spectra always are narrower than diamond.

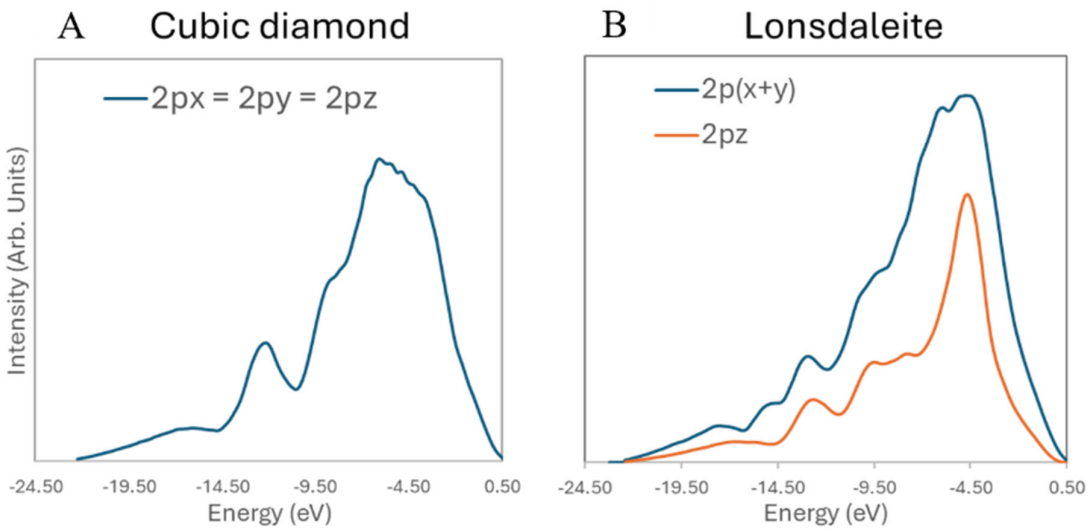

Figure 6. a) and b) Show theoretical calculation of DOS for cubic diamond and lonsdaleite, in the case of cubic diamond 2*px*, 2*py*, and 2*pz* are all equivalent. b) Lonsdaleite shows 2*px* and 2*py* are equivalent but 2*pz* is distinctly narrower. The theoretical calculations predict that one can differentiate cubic diamond from lonsdaleite using SXES spectroscopy of C-K.

5. CONCLUSIONS

Using an EPMA equipped with traditional WDS and EDS detectors, together with SXES, we have shown that this combination of detectors can characterise the main mineralogy through

the application of cluster analysis to group together with similar spectra and then identify the main minerals present. The SXES has been able to differentiate the different grain orientations and show that single graphite grains are dominated by a single orientation within a Tanzanian sample. These finding indicates that formation conditions were most likely sustained for long enough to fully graphitize any organic matter. T he sensitivity of the SXES to carbon makes it a good tool to examine these types of deposits.

Measurements on ureilite NWA 7983 have shown we can differentiation the formation of diamond and lonsdaleite from graphite at both the macro and nanoscale. By combining SXES with theoretical DOS calculations we have confirmed the presence of lonsdaleite/diamond intergrowths and shown when used in combination with other spectroscopies this is a powerful tool that enable new information to be gained from materials and minerals.

6. ACKNOWLEDGEMENT

The authors gratefully acknowledge funding from the ARC LE130100087.

7. REFERENCES

[1] MacRae C M, Pearce M A, Wilson N C, Torpy A, Glenn M A and Russo S P 2020 *Microsc. Microanal.* **26** 814-820
[2] Tomkins A G, Wilson N C, MacRae C, Salek A, Field M R, Brand H E A, Langendam A D, Stephen N R, Torpy A, Pintér Z, Jennings L A and McCulloch D G 2022 *Proc. Nat. Acad. Sci. USA* **119** e2208814119
[3] Fritz H, Abdelsalam M, Ali K A, Bingen B, Collins A S, Fowler A R, Ghebreab W, Hauzenberger C A, Johnson P R, Kusky T M, Macey P, Muhongo S, Stern R J and Viola G 2013 *J. Afr. Earth Sci.* **86** 65-106
[4] Ishii S, Terauchi M, Sato Y, Tamura N, Aono M and Abe H 2018 *Microscopy (Oxford)* **67** 244-249
[5] Srbinovsky J, Wilson N C, MacRae C M and Russo S P 2005 *J. Comput. Theor. Nanosci.* **2** 272-276
[6] Goodrich C A, Hartmann W K, O'Brien D P, Weidenschilling S J, Wilson L, Michel P and Jutzi M 2015 *Meteoritics Planet. Sci.* **50** 782-809
[7] Langendam A D, Tomkins A G, Evans K A, Wilson N C, MacRae C M, Stephen N R and Torpy A 2021 *Meteoritics Planet. Sci.* **56** 2062-2082
[8] Nakamuta Y and Toh S 2013 *Amer. Mineralogist* **98** 574-581
[9] Nemeth P, Garvie L A, Aoki T, Dubrovinskaia N, Dubrovinsky L and Buseck P R 2014 *Nature Commun.* **5** 5447
[10] Hanneman R E, Strong H M and Bundy F P 1967 *Science* **155** 995-997

[11] Bundy F P and Kasper J S 1967 *J. Chem. Phys.* **46** 3437-3446
[12] Bundy F P, Bassett W A, Weathers M S, Hemley R J, Mao H K and Goncharov A F 1996 *Carbon* **34** 141-153
[13] Turneaure S J, Sharma S M, Volz T J, Winey J M and Gupta Y M 2017 *Science Adv.* 3 eaao3561
[14] Irifune T, Kurio A, Sakamoto S, Inoue T and Sumiya H 2003 *Nature* **421** 599-600
[15] Pownceby M, MacRae C and Wilson N 2007 *Minerals Eng.* **20** 444-451
[16] MacRae C, Wilson N and Torpy A 2013 *Mineral. Petrol.* **107** 429-440
[17] Terauchi M, Koike M, Fukushima K and Kimura A 2010 *J. Electron Microsc. (Tokyo)* **59** 251-261
[18] MacRae C M, Hughes A E, Laird J S, Glenn A M, Wilson N C, Torpy A, Gibson M A, Zhou X, Birbilis N and Thompson G E 2018 *Microsc. Microanal.* **24** 325-341
[19] MacRae C M, Wilson N C, Torpy A and Hughes A E 2019 Microsc. Microanal. **25** 246-247
[20] Torpy A, Wilson N C, MacRae C M, Pownceby M I, Biswas P K, Rahman M A and Zaman M N 2020 *Microsc. Microanal.* **26** 768-792
[21] Dovesi R, Orlando R, Erba A, Zicovich-Wilson C M, Civalleri B, Casassa S, Maschio L, Ferrabone M, De La Pierre M, D'Arco P, Noël Y, Causà M, Rérat M and Kirtman B 2014 *Int. J. Quantum Chem.* **114** 1287-317
[22] Becke A D 1993 *J. Chem. Phys.* **98** 5648-5652
[23] Monkhorst H J and Pack J D 1976 *Phys. Rev. B* **13** 5188-5192
[24] Wilson N C, MacRae C M, Torpy A, Davidson C J and Vicenzi E P 2012 *Microsc. Microanal.* **18** 1303-1312
[25] Deer W A, Howie R A and Zussman J 1992 *An introduction to the rock-forming minerals. 2nd Edition*. [Twickenham, UK: Mineralogical Society of Great Britain and Ireland]
[26] Holliday J E 1968 *Soft X-ray band spectra*. (Fabian D J; Ed.) [London, UK: Academic Press] 101-132
[27] Teruachi M, Takahashi H, Takakura M, Murano T and Koshiya S 2019 *Handbook of soft X-ray emission spectra*. [Tokyo, Japan: JEOL Ltd.]
[28] Rai N, Downes H and Smith C 2020 *Geochem. Perspectives Lett.* **14** 20-25
[29] Ross A J, Steele A, Fries M D, Kater L, Downes H, Jones A P, Smith C L, Jenniskens P M, Zolensky M E and Shaddad M H 2011 *Meteoritics Planet. Sci.* **46** 364-378
[30] Nakamuta Y and Aoki Y 2000 *Meteoritics Planet. Sci.* **35** 487-493
[31] Nabiei F, Badro J, Dennenwaldt T, Oveisi E, Cantoni M, Hébert C, El Goresy A, Barrat J A and Gillet P 2018 *Nature Commun.* **9** 1327
[32] Nestola F, Goodrich C A, Morana M, Barbaro A, Jakubek R S, Christ O, Brenker F E, Domeneghetti M C, Dalconi M C, Alvaro M, Fioretti A M, Litasov K D, Fries M D, Leoni M, Casati N P M, Jenniskens P and Shaddad M H 2020 *Proc .Nat. Acad. Sci. USA* **117** 25310-25318
[33] Erba A, Desmarais J K, Casassa S, Civalleri B, Donà L, Bush I J, Searle B, Maschio L, Edith-Daga L, Cossard A, Ribaldone C, Ascrizzi E, Marana N L, Flament J P and Kirtman B 2022 *J. Chem. Theory Comput.* **19** 6891-6932